scientific reports

Check for updates

OPEN

Numerical approach towards gyrotactic microorganisms hybrid nanoliquid flow with the hall current and magnetic field over a spinning disk

Yu-Pei Lv[1], Ebrahem A. Algehyne[2], Maryam G. Alshehri[2], Ebraheem Alzahrani[3], Muhammad Bilal[4]✉, Muhammad Altaf Khan[5] & Muhammad Shuaib[4]

The article explores the effect of Hall current, thermal radiation, and magnetic field on hybrid nanofluid flow over the surface of a spinning disk. The motive of the present effort is to upgrade the heat transmission rate for engineering and industrial purposes. The hybrid nanofluids as compared to the conventional fluids have higher thermal properties. Therefore, in the present article, a special class of nanoparticles known as carbon nanotubes (CNTs) and iron ferrite nanoparticles are used in the base fluid. The system of modeled equations is depleted into dimensionless differential equations through similarity transformation. The transform equations are further solved through the Parametric Continuation method (PCM). For the parametric study, the physical parameters impact on velocity, energy, mass transmission, and motile microorganism's concentration profiles have been sketched. The obtained results are compared with the existing literature, which shows the best settlement. It concluded that the heat transmission rate reduces for Hall current and rises with radiative parameter. The results perceived that the addition of CNTs in carrier fluid is more efficacious than any other types of nanoparticles, due to its C–C bond. CNTs nanofluid can be more functionalized for the desired achievement, which can be utilized for a variety of applications by functionalization of non-covalent and covalent modification.

Abbreviations

u, v, w	Velocity component
T	Fluid temperature (K)
T_w	Temperature of the Surface
T_∞	Temperature at infinity
B_0	Magnetic field
Θ	Dimensionless temperature
$\tilde{N}$	Density of motile microorganism
σ^*	Stefan Boltzmann coefficient
$m = \omega_z \tau_z$	Hall current
ω_z	Frequency of electron
k_{hnf}	Thermal conductivity
ν_{hnf}	Nanofluid kinematic viscosity
ρ_{hnf}	Hybrid Nanofluid density
$\phi_1 = \phi_{CNT}$	Carbon nanotubes volume friction
PCM	Parametric continuation method

[1]Department of Mathematics, Huzhou University, Huzhou 313000, People's Republic of China. [2]Department of Mathematics, Faculty of Science, University of Tabuk, P.O. Box 741, Tabuk 71491, Saudi Arabia. [3]Department of Mathematics, Faculty of Science, King Abdulaziz University, P.O. Box 80203, Jeddah 21589, Saudi Arabia. [4]Department of Mathematics, City University of Science and Information Technology, Peshawar, Pakistan. [5]Institute for Groundwater Studies, Faculty of Natural and Agricultural Sciences, University of the Free South Africa, Bloemfontein, South Africa. ✉email: bilalchd345@gmail.com

Fe_3O_4	Iron oxide
$\rho_{Fe_3O_4}$	Density of iron oxide
$(\rho Cp)_{hnf}$	Volumetric heat capacity
p	Pressure
f, g	Dimensional velocity
Ω	Velocity angular of the disk
(r, φ, z)	Cylindrical coordinate
W_c	Cell swimming velocity
Φ	Dimensionless temperature
D_n	Microorganism diffusion
k^*	Mean absorption coefficient
qr	Radioactive heat flux
τ_z	Collision of electron
α_{hnf}	Electrical conductivity
μ_{hnf}	Dynamic viscosity of nanofluid
α_{hnf}	Thermal diffusivity
$\phi_2 = \phi_{Fe_3O_4}$	Iron oxide volume friction
CNTs	Carbon nanotubes
Pe	Peclet number
ρ_{CNT}	Density of carbon nanotubes
$(Cp)_{MS}$	Specific heat capacity
$\mathbb{C}_1, \mathbb{C}_2, \mathbb{C}_3, \mathbb{C}_4, \mathbb{C}_5,$	Dimensionless constant

The heat and mass transmission with nanofluid flow run over revolving disk have wide range implementation in the heat exchanger and electronic devices[1]. The applications of such type problems are in computer hardware for storage purpose, thermal energy generating system, electronic instruments, gas turbine, spinning devices, chemical processes, geothermal industry, various types of medical instruments, etc. The suction influence acts on the fluid flow over a revolving disk has been determined by Stuart[2]. Ahmadian et al.[3,4] reported the unsteady hybrid nanofluid flow with mass and energy transmission using the parametric continuation method (PCM) over a non-uniform spinning disk. They concluded that the addition of nanomaterial in the base fluid has a crucial role in hyperthermia, power generation and microfabrication. Shahid et al.[5] reported the influence of gyrotactic microorganism MHD nanofluid flow utilizing the local Linearization method. Bhatti et al.[6] introduced a theoretical approach about gyrotactic microorganism migratory in a blood-based fluid through a narrow artery. Hayat et al.[7] highlighted the heat transmission in Darcy-Forchemmier flow of cupper (*Cu*) and silver *(Ag)* nanofluid between the gap of two spinning stretchable disks. Muhammad et al.[8] scrutinized the unsteady flow of rheological Carreau microorganism nanofluid with thermal radiation and velocity slip over a moving wedge. Shuaib et al.[9] illustrated the frictional nature of viscous fluid flow over a flexible surface of a rotating disk with heat transport characteristics. Gul et al.[10] examined the thermal characteristics of hybrid nanofluid between the conical gap of disk and cone for different cases of disk-cone rotation.

Hannes Alfven[11] pioneered the field of MHD, for this work he won the Nobel Prize (1970) in the field of Physics. The basic principle of MHD is to regulate fluid flow. Some applications of MHD are mostly used in malignant tumours, arthritis, blood pressure, and brain therapy. Siddiqui et al.[12] investigated the MHD movement of liquid flow in a porous medium with application throughout the respiratory tract to monitor diseases. The MHD rotating boundary layer flow, over shrinking permeable surface was solved by the numerical procedure (Keller-box method) in Ref.[13]. Neeraja et al.[14] addressed MHD Casson liquid flow with convective boundary conditions and viscous dissipation over a deformable channel. The steady three-dimensional MHD Casson nanofluid flow between two spinning plates has been scrutinized by Refs.[15]. Maryam et al.[16] highlighted the unsteady MHD flow over a rotating porous surface of the hybrid liquid. Lokesh et al.[17] illustrated numerically the chemical reaction of the Casson nanofluid over an expanding surface with heat and mass transport. An unsteady three-dimensional MHD flow of nanofluid is investigated by Rauf et al.[18] as a result of the rotation of infinite disc with periodic oscillation dependent on time. A numerical evaluation of the MHD Casson liquid over a deformable substrate with slip conditions is studied by Murthy[19]. Oyelakin et al.[20] revealed the upshot of the velocity slip in a tangent hyperbolic nanofluid on the flow and heat transfer features. Khashi'ie et al.[21] investigated the flow and heat transmission characteristics of copper and aluminum oxide hybrid nanofluid over a radially shrinking surface with the MHD and Joule heating effect. Tlili et al.[22] scrutinized an MHD flow of hybrid nanofluid through a non-uniform stretched thick plane with slip effects.

The heat transfer in carbon-nanofluids has gotten extensive attention among researchers in different sectors of technologies. CNTs are the simple chemical structure along with the composition of carbon atoms, rolled in cylindrical form. CNTs have extraordinary thermophysical, chemical, electrical, and mechanical features that can be utilized easily as a nanoparticle in the base fluid. They have unique advantages on account of little size tube structure, such as large surface area, tube shape, configuration, chemical stability, hardness, and their smallest dimension over other nanoparticles. CNTs depend on the number of graphene layers, which subdivided it into single-walled & multi-walled carbon nanotubes, abbreviated as SWCNTs and MWCNTs respectively. Khan et al.[23] highlighted the physical aspects of entropy optimization within a rotating frame of carbon nanotubes (CNTs) in convective MHD effective flow. Anuar et al.[24] has evaluated the upshot of MHD on the steady, two-dimensional induced flow of carbon nanotubes via the nonlinear surface. The main intention of Ref.[25] is to examine the electrical MHD spinning flow of single and multi-walled nanotubes based on several types of carrier fluid. Mahanthesh[26] studied the carbon nanofluids flow passing via a revolving disk. The consequences of MHD

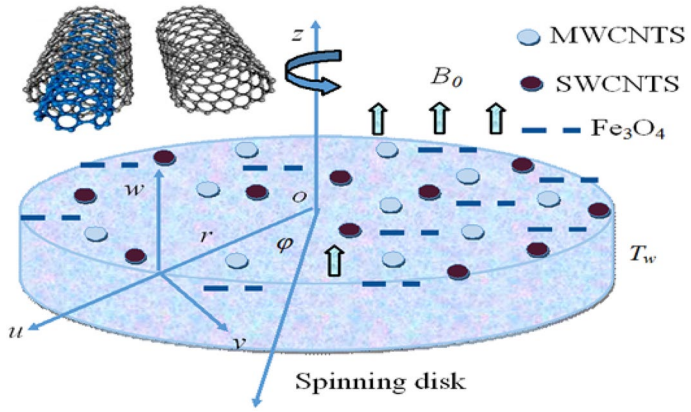

Figure 1. Spinning disk geometry.

on stagnation point flow having carbon nanotubes along stretch/shrink layer are studied by Anuar et al.[27]. Gul et al.[28] presented the numerical model, in order to compare and explore hybrid and simple nanomaterial effect over an extending sheet. Ahmed et al.[29] presented a novel model of the unstable MHD heat transmission flow over a shrinking surface in carbon nanotubes with variable viscosity. The MHD radiative and incompressible steady flow of Carreau nanofluid explored with carbon nanotubes are investigated by Nagalakshm & Vijaya[30]. Tulu and Ibrahim[31] scrutinized the carbon nanofluid flow with the result of Cattaneo–Christov heat flux model due to stretchable rotating disks. Both SWCNTs and MWCNTs are known as the base fluid of ethylene glycol. The physical prospects of hybrid nanofluid under the impact of thermal radiation and slip were presented by Ghadikolaei and Gholinia[32].

The motivation of current work is to explore the upshot of Hall current, carbon nanotubes, and iron ferrite nanofluid flow over a spinning disk under the effect of thermal radiation and magnetic field. The second priority is to extend the idea of Ref.[33] and enhance the thermophysical properties of carrier fluids. As compared to conventional fluids the study of hybrid nanofluids provides an extraordinary enhancement in heat and mass transmission and thermal conductivity. Therefore, we are taking nanofluid models, which are assembled of CNTs and Fe_3O_4 with base fluid water. The system of modeled equations is renovated into dimensionless differential equations through Karman's approach, which are further tacked through the Parametric Continuation method.

Mathematical Formulation

This segment highlights the physical background and mathematical terminology of the present hybrid nanofluid problem.

Physical description. In this study, we presume the steady hybrid nanofluid flow passes over a spinning disk. The insulated spinning disk is placed at z = 0, moving along the z-axis. The magnetic field B_0 is uniformly applied perpendicular to the disk surface. The disk is revolving with Ω (angular velocity). T and p correspond to the temperature and pressure of nanofluid. Hall current has been signified by $m = \tau_\varepsilon \omega_\varepsilon$, here ω_ε specifies the frequency of electron and τ_ε specifies collision of the electron where T_w and T_∞ are assumed as the temperature of the disk surface and away from the surface respectively. Figure 1 displays the geometry of the flow and cylindrical coordinate (r, φ, z) system.

Equation of motion. Based on the above assumption, the flow equations can be defined as[33–35]:

$$\frac{\partial u}{\partial r} + \frac{u}{r} + \frac{\partial w}{\partial z} = 0, \tag{1}$$

$$\rho_{hnf}\left(u\frac{\partial u}{\partial r} + w\frac{\partial u}{\partial z} - \frac{v^2}{r}\right) + \frac{\partial p}{\partial r} = \mu_{hnf}\left(\frac{\partial^2 u}{\partial r^2} - \frac{u}{r^2} + \frac{1}{r}\frac{\partial u}{\partial r} + \frac{\partial^2 u}{\partial z^2}\right) - \frac{\sigma_{hnf}B_0{}^2}{(1+m^2)}(u - mv), \tag{2}$$

$$\rho_{hnf}\left(u\frac{\partial v}{\partial r} + w\frac{\partial v}{\partial z} - \frac{uv}{r}\right) = \mu_{hnf}\left(\frac{\partial^2 v}{\partial r^2} - \frac{v}{r^2} + \frac{1}{r}\frac{\partial v}{\partial r} + \frac{\partial^2 v}{\partial z^2}\right) - \frac{\sigma_{hnf}B_0{}^2}{(1+m^2)}(u - mv), \tag{3}$$

$$\rho_{hnf}\left(u\frac{\partial w}{\partial r} + w\frac{\partial w}{\partial z}\right) + \frac{\partial p}{\partial z} = \mu_{hnf}\left(\frac{\partial^2 w}{\partial r^2} + \frac{\partial^2 w}{\partial z^2} + \frac{1}{r}\frac{\partial w}{\partial r}\right), \tag{4}$$

$$(\rho Cp)_{hnf}\left(u\frac{\partial T}{\partial r}+w\frac{\partial T}{\partial z}\right)=k_{hnf}\left(\frac{\partial^2 T}{\partial r^2}+\frac{\partial^2 T}{\partial z^2}+\frac{1}{r}\frac{\partial T}{\partial r}\right)-\frac{\partial qr}{\partial z}, \tag{5}$$

$$\left(u\frac{\partial C}{\partial r}+w\frac{\partial C}{\partial z}\right)=D_{hnf}\frac{\partial^2 C}{\partial z^2}, \tag{6}$$

$$\left(w\frac{\partial \tilde{N}}{\partial z}+\tilde{w}\frac{\partial \tilde{N}}{\partial z}+\tilde{N}\frac{\partial \tilde{w}}{\partial z}\right)=D_n\frac{\partial^2 \tilde{N}}{\partial z^2}. \tag{7}$$

Here, (u, v, w),μ_{hnf} α_{hnf}, σ_{hnf} and ρ_{hnf} denoting the velocity component, dynamic viscosity, thermal diffusivity, electrical conductivity, and density of hybrid nanofluid. $\tilde{N}$ is the density motile of microorganisms, D_n is the microorganism diffusion and Wc shows the swimming speed of maximum cell respectively. The thermal conductivity and volumetric heat capacity are represented through k_{hnf} and $(\rho C_p)_{hnf}$ of the hybrid nanofluid, respectively. While qr is the radioactive heat flux and can be simply expressed as[36]:

$$qr=-\frac{4\sigma^*}{3k^*}.\frac{\partial T^4}{\partial z}, \tag{8}$$

Here, σ^* and k^* are the Stefan Boltzmann and mean absorption coefficient respectively.

Boundary conditions. The boundary conditions are:

$$u=0,\ v=\Omega\ r,\ T=T_w,\ \tilde{N}=\tilde{N}_w,\ C=C_w,\quad \text{at}\quad z=0,$$

$$u\to 0,\ v\to 0,\ T\to T_\infty,\ P=P_\infty,\ \tilde{N}\to\tilde{N}_\infty,\ C\to C_\infty\quad \text{at}\quad z\to\infty. \tag{9}$$

Similarity conversion. To transform the system of PDEs, we defined the following variables as[37]:

$$v=r\Omega g, u=r\Omega f', w=-\sqrt{r\Omega v_f}f, \Theta(\eta)=\frac{T-T_\infty}{T-T_w},$$

$$P=P_\infty+2\Omega v_f P(\eta), \eta=\sqrt{\frac{2\Omega}{v_f}}z, \Phi=\frac{C-C_\infty}{C_w-C_\infty}.h=\frac{n-n_\infty}{n_w-n_\infty}. \tag{10}$$

Now, by using Eq. (8) in Eqs. (1)–(7), we receive

$$2f'''+\frac{\mathbb{C}_1}{\mathbb{C}_4}\left(2ff''-f'^2+g^2\right)-\frac{\mathbb{C}_5}{\mathbb{C}_4}\frac{M}{\left(1+m^2\right)}\left(f'-mg\right)=0, \tag{11}$$

$$2g''+\frac{\mathbb{C}_1}{\mathbb{C}_4}\left(2fg'-2f'g\right)-\frac{\mathbb{C}_5}{\mathbb{C}_4}\frac{M}{\left(1+m^2\right)}\left(g+mf'\right)=0, \tag{12}$$

$$\frac{1}{\mathrm{Pr}}\Theta''\left(1+\frac{4N}{3}\right)+\frac{\mathbb{C}_2}{\mathbb{C}_3}f\Theta'=0, \tag{13}$$

$$\Phi''-Sc\left(f\Phi'\right)=0, \tag{14}$$

$$h''+\mathrm{Re}\left(2Scfh'+Pe\left(h'\Phi'-h\Phi''\right)\right)=0, \tag{15}$$

where

$$\mathbb{C}_1=\frac{\rho_{hnf}}{\rho_f}, \mathbb{C}_2=\frac{(\rho Cp)_{hnf}}{(\rho Cp)_f}, \mathbb{C}_3=\frac{k_{hnf}}{k_f}, \mathbb{C}_4=\frac{\mu_{hnf}}{\mu_f}, \mathbb{C}_5=\frac{\sigma_{hnf}}{\sigma_f}.$$

Here, $\mathbb{C}_1$, $\mathbb{C}_2$, $\mathbb{C}_3$, $\mathbb{C}_4$, $\mathbb{C}_5$ are the dimensionless constants.
The boundary conditions also transform as:

$$\begin{aligned} &f'=f=0,\ g=\Phi=\Theta=1,\ h=1\ \text{ at } \eta=0,\\ &f'\to 0, \Theta\to 0, \Phi\to 0, g\to 0,\ h=0 \text{ as } \eta\to\infty. \end{aligned} \tag{16}$$

Thermo-physical properties. The thermal properties of hybrid nanofluid are expressed as[38]:

$$\upsilon_{hnf} = \frac{\mu_{hnf}}{\rho_{hnf}}, \mu_{hnf} = \frac{\mu_f}{(1-\phi_1)^{5/2}(1-\phi_2)^{5/2}}, \frac{(\rho)_{hnf}}{(\rho)_f} = (1-\phi_2)\left\{1-\left(1-\frac{(\rho)Ms}{(\rho)_f}\right)\phi_1\right\} + \frac{(\rho)_{CNT}}{(\rho)_f}\phi_2,$$
$$\frac{(\rho C_p)_{hnf}}{(\rho C_p)_f} = (1-\phi_2)\left\{1-\left(1-\frac{(\rho C_p)Ms}{(\rho C_p)_f}\right)\phi_1\right\} + \frac{(\rho C_p)_{CNT}}{(\rho C_p)_f}\phi_2,$$
$$\frac{k_{hnf}}{k_{bf}} = \frac{1-\phi_2+2\phi_2\frac{k_{CNT}}{(k_{CNT}-k_{bf})}-\ln\frac{k_{CNT}+k_{bf}}{2k_{bf}}}{1-\phi_2+2\phi_2\frac{k_{bf}}{(k_{CNT}-k_{bf})}-\ln\frac{k_{CNT}+k_{bf}}{2k_{bf}}}, \frac{k_{bf}}{k_f} = \frac{k_{MS}+(m-1)_{kf}-(m-1)\phi_1(k_f-k_{MS})}{k_{MS}+(m-1)_{kf}-\phi_1(k_f-k_{MS})}. \tag{17}$$

Here,$(C_p)_{MS}$, ρ_{MS} and ρ_{CNT} specified specific heat capacities and densities of Fe_3O_4 and CNTs, respectively.

The constant terms of our calculation are radiation parameter, Prandtl number, Lewis number, Hartmann number, Schmidt number, and Peclet number:

$$N = \frac{4\sigma^* {T_\infty}^3}{\kappa^*\kappa_f}, \ \Pr = \frac{\mu_f(\rho Cp)_f}{\rho_f\kappa_f}, \ Le = \frac{\nu_{hnf}}{D_B}, \ M^2 = \frac{\sigma_f {B_0}^2}{\rho_f\Omega}, \ Sc = \frac{\upsilon_f}{D_f}, \ \mathrm{Pe} = \frac{bW_c}{D_n}. \tag{18}$$

The Skin friction, Sherwood numbers, and Nusselt Number are rebounded as[39]:

$$C_f = \frac{\sqrt{\tau_{wr}^2+\tau_{w\phi}^2}}{\rho_f(\Omega r)^2}, \ Sh = \frac{rj_w}{D_f(C_w-C_\infty)}, \ Nu = \frac{rq_w}{k_f(T_w-T_\infty)}, \tag{19}$$

where τ_{wr},$\tau_{w\phi}$, q_w and j_w stand for radial stress, transverse shear stress, heat flux at and mass flux at the surface of the disk, respectively.

$$\tau_{wr} = \left[\mu_{hnf}\left(\frac{du}{dz}+\frac{dw}{d\phi}\right)\right]_{z=0}, \tau_{w\phi} = \left[\mu_{hnf}\left(\frac{dv}{dz}+\frac{1}{r}\frac{dw}{d\phi}\right)\right]_{z=0}, q_w = -\frac{k_{hnf}}{k_f}\left(\frac{dT}{dz}\right)_{z=0}, j_w = -D_{hnf}\left(\frac{dC}{dz}\right)_{z=0}. \tag{20}$$

The drag force and heat transmission rate in dimensionless form are stated as:

$$\mathrm{Re}^{\frac{1}{2}}C_f = \frac{\sqrt{(G'(0))^2+(F'(0))^2}}{(1-\phi_1)^{2.5}(1-\phi_2)^{2.5}}, \mathrm{Re}^{\frac{-1}{2}}Nu = -\frac{k_{hnf}}{k_f}\Theta'(0), \mathrm{Re}^{\frac{-1}{2}}Sh = -\Phi'(0), \ \mathrm{Re} = \frac{\Omega r^2}{\upsilon_f}. \tag{21}$$

Problem solution

For the results, the system of Eqs. (10–13) is depleted to the first order by the following procedure, which is further solved through the Parametric Continuation method (PCM):

$$\left.\begin{aligned}&\eta=\zeta_1,\ f=\zeta_2,\ f'=\zeta_3,\ f''=\zeta_4,\ g=\zeta_5,\ g'=\zeta_6,\\&\Theta=\zeta_7,\ \Theta'=\zeta_8,\ \Phi=\zeta_9,\ \Phi'=\zeta_{10},\ h=\zeta_{11},\ h=\zeta_{12},\end{aligned}\right\} \tag{22}$$

$$\left\{\begin{aligned}&\zeta'=1,\ \ \zeta'_2=\zeta_3,\ \ \zeta'_3=\zeta_4,\\&\zeta'_4=\frac{\mathbb{C}_5}{2\mathbb{C}_4}\frac{M}{(1+m^2)}(\zeta_3-m\zeta_5)\frac{\mathbb{C}_1}{2\mathbb{C}_4}\left(2\zeta_2\zeta_4-{\zeta_3}^2+{\zeta_5}^2\right),\\&\zeta'_5=\zeta_6,\ \zeta'_6=\frac{\mathbb{C}_5}{2\mathbb{C}_4}\frac{M}{(1+m^2)}(\zeta_5-m\zeta_3)\frac{\mathbb{C}_1}{\mathbb{C}_4}(\zeta_2\zeta_6-\zeta_3\zeta_5),\\&\zeta'_7=\zeta_8,\ \ \zeta'_8=-\Pr\left(\frac{\mathbb{C}_3}{\mathbb{C}_4}\zeta_2\zeta_8\right)/1+\frac{4N}{3},\\&\zeta'_9=\zeta_{10},\ \zeta'_{10}=Sc(\zeta_2\zeta_{10}),\ \zeta'_{11}=\zeta_{12},\\&\zeta'_{12}=-\mathrm{Re}\left(2Sc\zeta_2\zeta_{12}+\mathrm{Pe}\left(\zeta_{12}\zeta_{10}-\zeta_{12}\zeta'_{10}\right)\right).\end{aligned}\right. \tag{23}$$

$$\left.\begin{aligned}&\zeta_2=\zeta_4=0,\ \zeta_5=1,\ \zeta_7=\zeta_9=1,\ \zeta_{10}=1 \text{ at } \eta=0,\\&\zeta_3\to 0,\ \zeta_5\to 0,\ \zeta_7\to 0,\ \zeta_9\to 0,\ \zeta_9\to 0 \text{ as } \eta\to\infty.\end{aligned}\right\} \tag{24}$$

Results and discussion

The discussion section scrutinizes the behavior of velocity, temperature, and motile microorganism's concentration distributions against the variation of several physical constraints for hybrid nanofluid consist of CNTS and magnetic ferrite nanoparticles. The outputs are revealed through the comparative Figs. 2, 3, 4, 5, 6, 7 and Tables. The thermophysical characteristics are given in Table 1. To validate and ensure our results, we have plotted Table 2 for the numerical outcomes $f''(0)$,$-g'(0)$,$-\Theta'(0)$ and $-\Phi'(0)$ to compare it with published work (Refs.[33,38,39]), which show the best agreement. The influence of magnetic parameter M, volume fraction ϕ_2 and rotation parameter Ω versus shear stresses are scrutinized in Tables 3 and 4. It has been observed that with increment in magnetic parameter M, volume fraction ϕ_2 and rotation parameter Ω, the positive changes occurred in $f''(0)$ and $-g'(0)$, consequently the drag forces enhances. The effect of Ω, ϕ_1, ϕ_2, Pr and N against

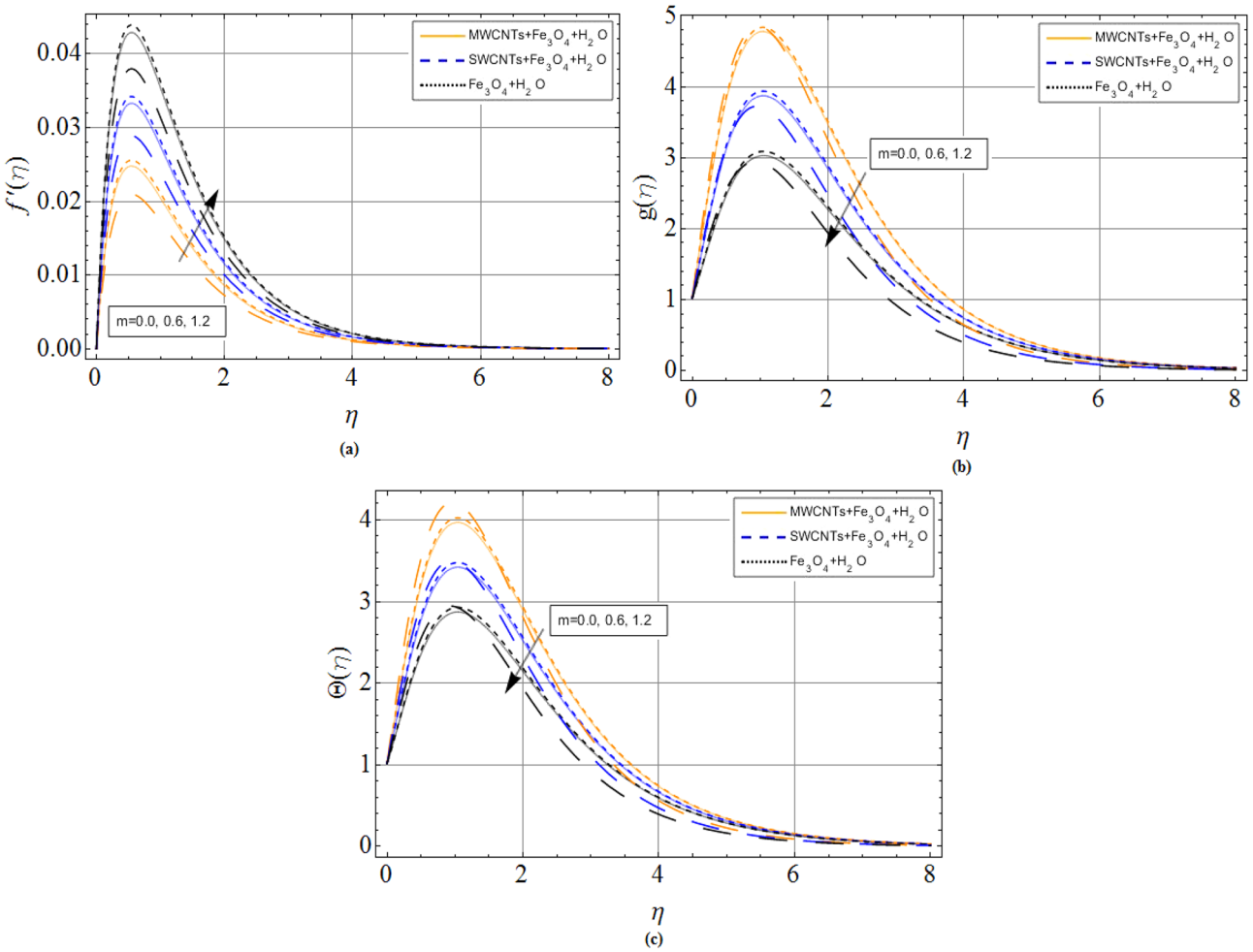

Figure 2. Hall current parameter m effect on (**a**) axial velocity $f'(\eta)$ (**b**) radial velocity $g(\eta)$ (**c**) temperature $\Theta(\eta)$. When $\phi_1 = 0.01, \phi_2 = 0.2, Sc = 2.0, Pr = 6.2, M = 1.0. N = 0.4$.

heat transfer rate are drawn via Table 5. The improving credit of volume friction parameters (ϕ_1, ϕ_2) declines the Nusselt number, which also results in enhances the fluid temperature of both iron oxide and CNTs nanofluid. The numerical outcomes for Sherwood number $-\Phi'(0)$ against volume friction parameters (ϕ_1, ϕ_2) and Schmidt number are discussed in Table 6.

The flow mechanism and coordinate geometry are exhibited in Fig. 1. From Fig. 2a–c, we perceive that the increasing effects of Hall current parameter m enlarge the axial velocity $f'(\eta)$. Physically, $\left(\sigma_{hnf}/1 + m^2\right)$ electrical conductivity enhances with rising credit of m, which declines the damping impact of M on axial velocity $f'(\eta)$. Thus, slightly away from the disk surface $(\eta \approx 5.0)$, both fluids achieved their peak velocity Fig. 2a while an opposite trend has been observed in Fig. 2b,c. Because radial velocity $g(\eta)$ and temperature profiles $\Theta(\eta)$ are reduced with the variation of Hall current parameter m. The axial velocity $f'(\eta)$ and radial velocity $g(\eta)$ profiles of hybrid nanofluid decline against the growing effects of magnetic strength M, due to the resistive effect created by magnetic strength shown in Fig. 3a,b. While this opposing force also produces some heat energy, which enhances fluid temperature $\Theta(\eta)$ illustrated through Fig. 3c.

Figures 4a–c and 5a–c are sketched for the purpose to display the upshot of volume fraction parameters (ϕ_1, ϕ_2), where ϕ_1 expresses single and multi-wall carbon nanotubes quantities and ϕ_2 expresses iron ferrite Fe_3O_4 quantities, versus axial velocity $f'(\eta)$, radial and temperature profiles, respectively. It can be concluded that the rising credit of ϕ_1 and ϕ_2 reduces specific heat capacity of the base fluid, while on other hand the variation of volume friction parameters increase the thermal expansion rate, as a result, the velocity and temperature of fluid improve, respectively.

Figure 6a,b revealed the influence of thermal radiation parameter N and Prandtl number Pr on temperature profile $\Theta(\eta)$, respectively. The fluid temperature enhances with the variation of thermal radiation, while declines with Prandtl effects. The heat energy radiated from the disk surface enhances the kinetic energy of fluid, which causes the rises in velocity as well as the temperature of the fluid. On the other hand, high Prandtl fluid has always greater specific heat capacity and kinematic viscosity, which affects fluid temperature to reduce. The influence of Lewis number Le and Peclet number Pe versus motile microorganism's concentration profile $h(\eta)$ have been shown through Fig. 6c,d. The rising credit of Lewis's number reduces molecular diffusion rate, which causes

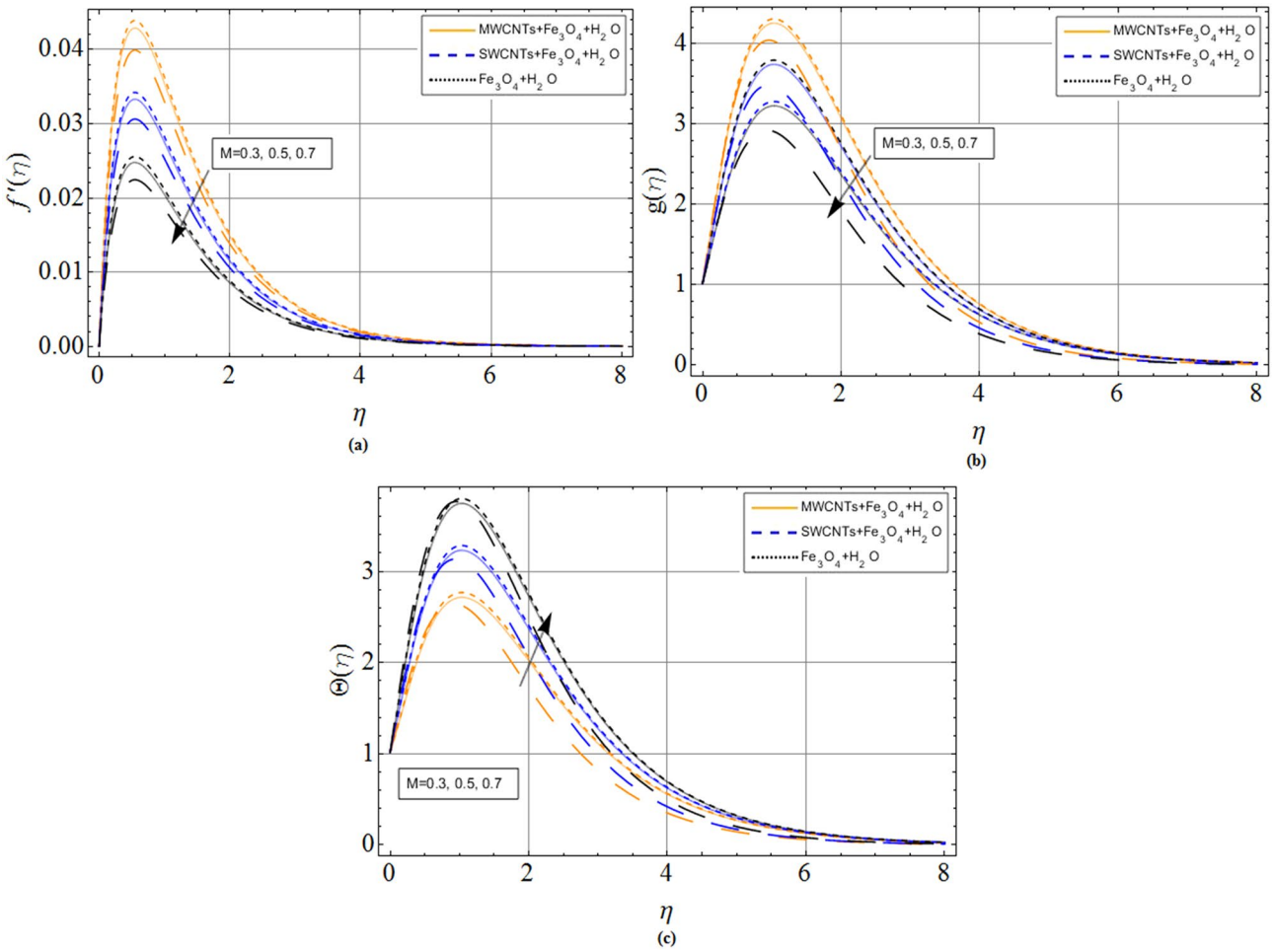

Figure 3. Magnetic parameter M effect on (**a**) axial velocity $f'(\eta)$ (**b**) radial velocity $g(\eta)$ (**c**) temperature $\Theta(\eta)$. When $\phi_1 = 0.01, \phi_2 = 0.2, Sc = 2.0, Pr = 6.2, M = 1.0, N = 0.5$.

increases in motile microorganism's concentration profile $h(\eta)$ Fig. 6c. Similarly, microorganism diffusion also reduces versus growing values of Peclet number Fig. 6d.

From Fig. 7, we perceive that mass transfer rate declines with positive increments of Schmidt number Sc. Physically, $Sc = \nu_f / D_f$ the rising trend of Schmidt number improves the kinematic viscosity of carrier fluid, which decreases the mass transfer rate.

Conclusion

The intention of the present work to investigate the upshot of Hall current on *CNTs* and iron ferrite hybrid nanofluid flow over a spinning disk under the influence of thermal radiation and magnetic field. Improving the heat transmission rate for engineering and industrial purposes is the motivation of the present work. Therefore, the present problem is modeled in form of PDEs, which are further depleted through similarity transformation. The transform equations are solved through the Parametric Continuation method (PCM) for the numerical results. The key points are rebounded as:

- The inclusion of (CNTs) and Fe_3O_4 nanoparticles in base fluid positively affect heat and mass transmission.
- The opposing effect generated due to the Lorentz force is responsible for the decrease of axial $f'(\eta)$ and radial velocity $g(\eta)$ profiles. While an opposite trend has been observed between temperature and magnetic strength because the same retarding effect produces heat due to friction forces, which enhances the fluid temperature.
- The influence of Lewis number Le and Peclet number Pe both enhance the motile microorganism's concentration profile $h(\eta)$. Because, the increasing values of Lewis number reduces the molecular diffusion rate, which increases the motile microorganism's concentration profile $h(\eta)$.
- The positive effects of Hall current parameter m enlarge the axial velocity $f'(\eta)$. Physically, $\sigma_{hnf}/1 + m^2$ effective conductivity reduces with rising values of m, which declines the damping impact of M axial velocity $f'(\eta)$. Thus, slight away from the disk surface ($\eta \approx 5.0$), both types of nanofluid achieved their peak velocity

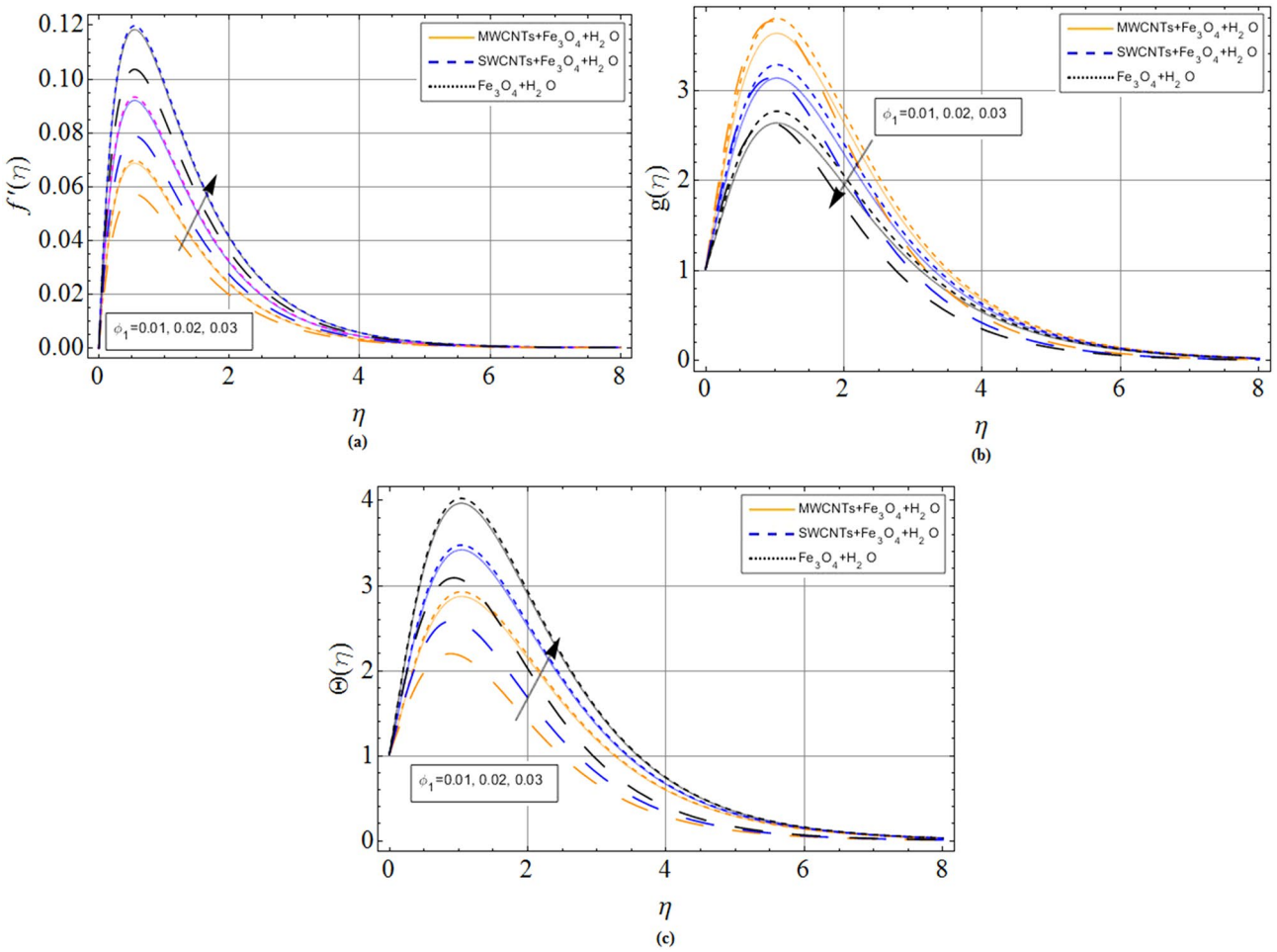

Figure 4. Volume friction parameter $\phi_1(CNTs)$ effect on (**a**) axial velocity $f'(\eta)$ (**b**) radial velocity $g(\eta)$ (**c**) temperature $\Theta(\eta)$. When $\phi_1 = 0.01, \phi_2 = 0.2, Sc = 2.0, Pr = 6.2, M = 1.0, N = 0.5$.

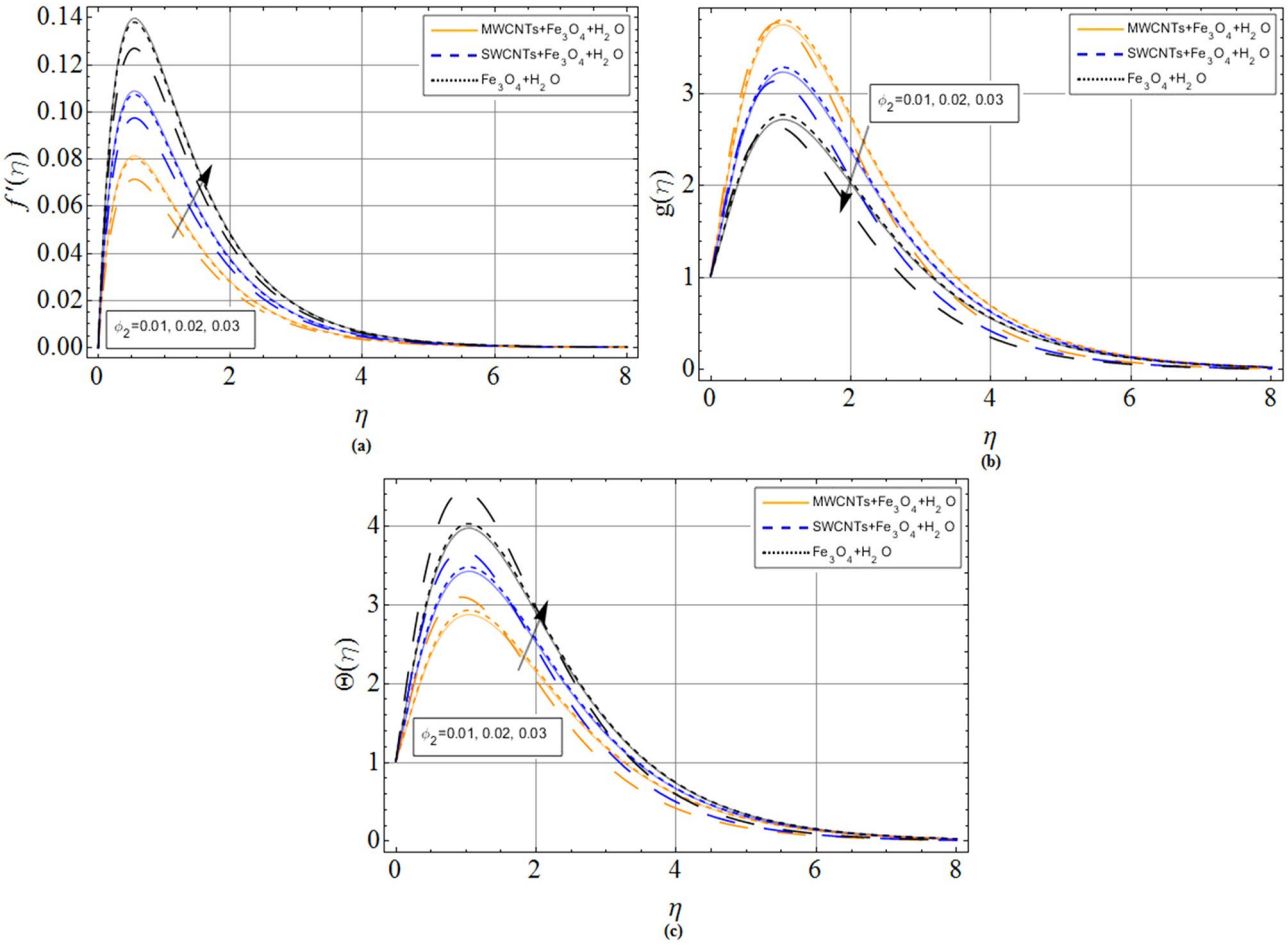

Figure 5. Volume friction parameter $\phi_2(Fe_3O_4)$ effect on (**a**) axial velocity $f'(\eta)$ (**b**) radial velocity $g(\eta)$ (**c**) temperature $\Theta(\eta)$. When $\phi_1 = 0.01, \phi_2 = 0.2, Sc = 2.0, Pr = 6.2, M = 1.0, N = 0.5$.

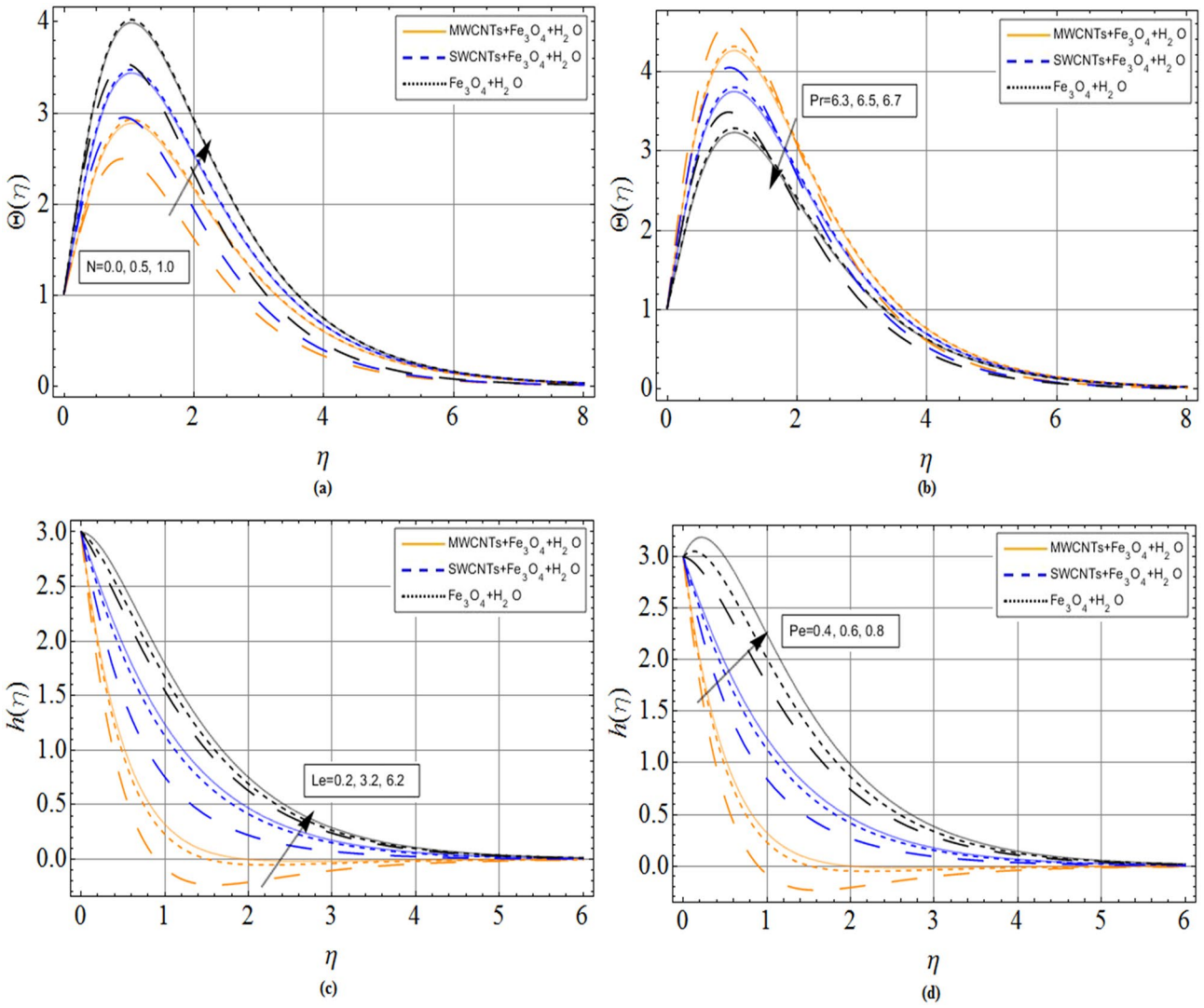

Figure 6. (**a**) Radiation parameter N (**b**) Prandtl number Pr (**c**) Lewis number Le (**d**) Peclet number Pe effect on temperature $\Theta(\eta)$ and Motile microorganisms' concentration $h(\eta)$ profiles respectively. When $\phi_1 = 0.01, \phi_2 = 0.2, Sc = 2.0, Pr = 6.2, M = 1.0, N = 0.5$.

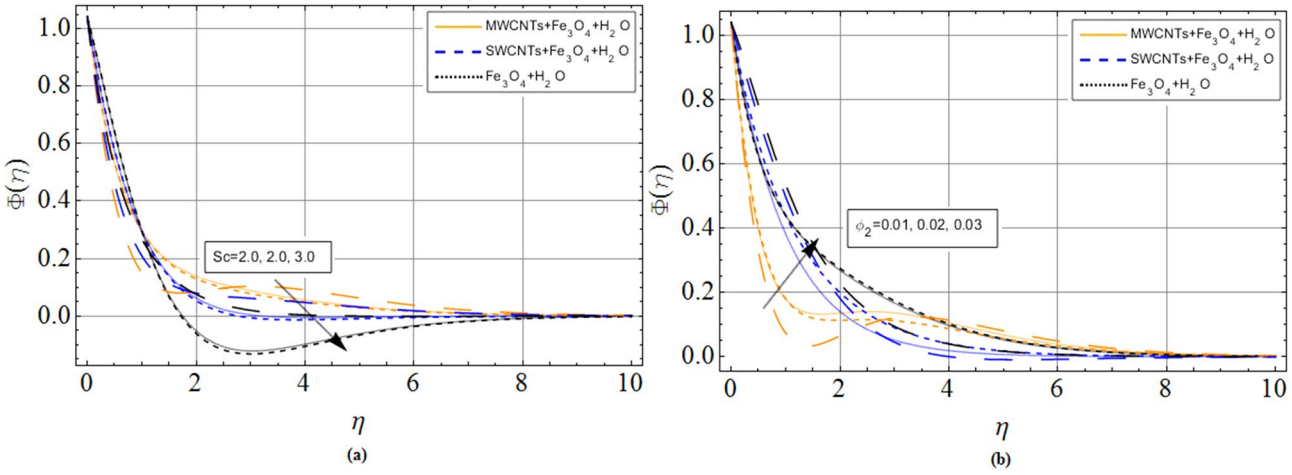

Figure 7. (**a**) Schmidt number Sc effects on concentration profile $\Phi(\eta)$ (**b**) volume friction parameter effects concentration profile $\Phi(\eta)$. When $\phi_1 = 0.01, Pr = 6.2, M = 1.0, N = 0.5$.

	$\rho(kg/m^3)$	$C_p(j/kgK)$	$k(W/mK)$
Pure water	997.1	4179	0.613
SWCNTs	2600	425.0	6600
MWCNTs	1600	796.0	300.0
Fe_3O_4	5200	670.0	6.00

Table 1. The numerical properties of water, *CNTs* and Fe_3O_4 .

	Yin et al.[38]	Acharya et al.[33]	Refs.[39]	Present work
$f''(0)$	0.51022941	0.5102295	–	0.5102297
$-g'(0)$	0.61591990	0.6159197	–	0.615199
$-\Theta'(0)$	0.93387285	0.9338728	–	0.9338731
$-\Phi'(0)$	–	–	−0.78555	−0.78555

Table 2. The numerical of $f''(0), -g'(0), -\Theta'(0)$, and $-\Phi'(0)$, when $\phi_1 = \phi_2 = 0.5$, $Pr = 6.2$, $N = 0.5$ and $M = 2.0$.

Ω	M	ϕ_2	$\frac{f''(0)}{(1-\phi_1)^{2.5}(1-\phi_2)^{2.5}}$ Fe_3O_4	$\frac{f''(0)}{(1-\phi_1)^{2.5}(1-\phi_2)^{2.5}}$ *SWCNTs*	$\frac{f''(0)}{(1-\phi_1)^{2.5}(1-\phi_2)^{2.5}}$ *MWCNTs*
2	2	0.2	0.473164	0.385087	0.371700
3			0.512794	0.477838	0.455406
4			0.548806	0.477798	0.496049
	3		0.563014	0.482898	0.496116
	4		0.564584	0.484453	0.497016
		0.3	0.578366	0.491306	0.497911
		0.4	0.591749	0.497773	0.498412

Table 3. The numerical outcomes for skin friction $(1-\phi_1)^{2.5}(1-\phi_2)^{2.5}f''(0)$ when $\phi_1 = \phi_2 = 0.5$, $Pr = 6.2$, $N = 0.5$ and $M = 2.0$.

Ω	M	ϕ_2	$\frac{g'(0)}{(1-\phi_1)^{2.5}(1-\phi_2)^{2.5}}$ Fe_3O_4	$\frac{g'(0)}{(1-\phi_1)^{2.5}(1-\phi_2)^{2.5}}$ *SWCNTs*	$\frac{g'(0)}{(1-\phi_1)^{2.5}(1-\phi_2)^{2.5}}$ *MWCNTs*
2	2	0.2	−0.63129	−0.48356	−0.43156
3			−−0.68588	−0.58340	−0.58522
4			−1.71301	−0.64021	−1.64321
	3		−0.71862	−0.73153	−0.69853
	4		−0.76631	−0.81881	−0.76681
		0.3	−0.77488	−0.83194	−0.87494
		0.4	−1.78431	−0.88149	−0.88432

Table 4. The numerical outcomes for skin friction $\frac{g'(0)}{(1-\phi_1)^{2.5}(1-\phi_2)^{2.5}}$ when $\phi_1 = \phi_2 = 0.5$, $Pr = 6.2$, $N = 0.5$ and $M = 2.0$.

Ω	ϕ_1	ϕ_2	Pr	N	$-\left(\frac{k_{hnf}}{k_{nf}}\right)\Theta'(0)$	$-\left(\frac{k_{hnf}}{k_{nf}}\right)\Theta'(0)$	$-\left(\frac{k_{hnf}}{k_{nf}}\right)\Theta'(0)$
					Fe_3O_4	SWCNTs	MWCNTs
2	0.02	0.2	6.2	0.2	− 0.470880	− 0.357508	− 0.358063
3					− 0.281709	− 0.271003	− 0.272758
4					− 0.161703	− 0.123278	− 0.128023
	0.03				− 0.139423	− 0.017846	− 0.020162
	0.04				− 0.299640	− 0.011775	− 0.016102
		0.3			− 0.140306	− 0.325440	− 0.305060
		0.4			− 0.610370	− 0.176231	− 0.149620
			6.6		− 1.802850	− 0.508730	− 2.036413
			7.0		− 0.685082	− 0.631178	− 2.129232
				0.3	− 0.232681	− 0.216310	− 1.109990
				0.4	− 0.221650	− 0.110080	− 1.074766

Table 5. The outcomes for Nusselt number $-\left(\frac{k_{hnf}}{k_{nf}}\right)\Theta'(0)$ when $\phi_1 = \phi_2 = 0.5$, $Pr = 6.2$, $N = 0.5$ and $M = 2.0$.

ϕ_1	ϕ_2	Sc	$-\Phi'(0)$	$-\Phi'(0)$	$-\Phi'(0)$
			Fe_3O_4	SWCNTs	MWCNTs
0.02	0.2	0.3	− 0.615955	− 0.621530	− 0.621800
0.03			− 0.643492	− 0.649438	− 0.649887
0.04			− 1.673735	− 0.674350	− 0.674620
	0.3		− 0.694710	− 0.695040	− 0.696122
	0.4		− 0.712402	− 0.717622	− 0.718961
		0.4	− 0.728808	− 0.725706	− 0.7375141
		0.5	− 1.784112	− 0.731965	− 0.770660

Table 6. The numerical outcomes for Sherwood number $-\Phi'(0)$.

Data availability

The data that support the findings of this study are available from the corresponding author upon reasonable request.

Received: 20 December 2020; Accepted: 9 April 2021
Published online: 26 April 2021

References

1. Ma, Y., Mohebbi, R., Rashidi, M. & Yang, Z. Study of nanofluid forced convection heat transfer in a bent channel by means of lattice Boltzmann method. *Phys. Fluids* **30**(3), 032001 (2018).
2. Stuart, J. On the effects of uniform suction on the steady flow due to a rotating disk. *Quart. J. Mech. Appl. Math.* **7**(4), 446–457 (1954).
3. Ahmadian, A., Bilal, M., Khan, M. A. & Asjad, M. I. The non-Newtonian maxwell nanofluid flow between two parallel rotating disks under the effects of magnetic field. *Sci. Rep.* **10**(1), 1–14 (2020).
4. Ahmadian, A., Bilal, M., Khan, M. A. & Asjad, M. I. Numerical analysis of thermal conductive hybrid nanofluid flow over the surface of a wavy spinning disk. *Sci. Rep.* **10**(1), 1–13 (2020).
5. Shahid, A., Huang, H., Bhatti, M. M., Zhang, L. & Ellahi, R. Numerical investigation on the swimming of gyrotactic microorganisms in nanofluids through porous medium over a stretched surface. *Mathematics* **8**(3), 380 (2020).
6. Bhatti, M. M., Marin, M., Zeeshan, A., Ellahi, R. & Abdelsalam, S. I. Swimming of motile gyrotactic microorganisms and nanoparticles in blood flow through anisotropically tapered arteries. *Front. Phys.* **8**, 95 (2020).
7. Hayat, T., Nazar, H., Imtiaz, M. & Alsaedi, A. Darcy-Forchheimer flows of copper and silver water nanofluids between two rotating stretchable disks. *Appl. Math. Mech.* **38**(12), 1663–1678 (2017).
8. Muhammad, T., Alamri, S. Z., Waqas, H., Habib, D. & Ellahi, R. Bioconvection flow of magnetized Carreau nanofluid under the influence of slip over a wedge with motile microorganisms. *J. Therm. Anal. Calorim.* **143**(2), 945–957 (2021).
9. Shuaib, M., Bilal, M., Khan, M. A. & Malebary, S. J. Fractional analysis of viscous fluid flow with heat and mass transfer over a flexible rotating disk. *Comput. Model. Eng. Sci.* **123**(1), 377–400 (2020).
10. Gul, T., Bilal, M., Alghamdi, W., Asjad, M. I. & Abdeljawad, T. Hybrid nanofluid flow within the conical gap between the cone and the surface of a rotating disk. *Sci. Rep.* **11**(1), 1–19 (2021).
11. Alfvén, H. Existence of electromagnetic-hydrodynamic waves. *Nature* **150**(3805), 405–406 (1942).
12. Siddiqui, A., Manzoor, N., Maqbool, K., Mann, A. B. & Shaheen, S. Magnetohydrodynamic flow induced by ciliary movement: An application to lower respiratory track diseases. *J. Magn. Magn. Mater.* **480**, 164–170 (2019).
13. Hafidzuddin, M. E. H., Nazar, R. & Arifin, N. Application of the Keller-box method to magnetohydrodynamic rotating flow over a permeable shrinking surface. *Embrac. Math. Divers.* **36**, 2 (2019).
14. Neeraja, A., Devi, R. R., Devika, B., Radhika, V. N. & Murthy, M. K. Effects of viscous dissipation and convective boundary conditions on magnetohydrodynamics flow of casson liquid over a deformable porous channel. *Results Eng.* **4**, 100040 (2019).

15. Zubair, M. *et al.* Entropy generation optimization in squeezing magnetohydrodynamics flow of casson nanofluid with viscous dissipation and joule heating effect. *Entropy* **21**(8), 747 (2019).
16. Subhani, M. & Nadeem, S. Numerical investigation into unsteady magnetohydrodynamics flow of micropolar hybrid nanofluid in porous medium. *Phys. Scr.* **94**(10), 105220 (2019).
17. Lokesh, H. J., Gireesha, B. J. & Kumar, K. G. Characterization of chemical reaction on magnetohydrodynamics flow and nonlinear radiative heat transfer of Casson nanoparticles over an exponentially sheet. *J. Nanofluids* **8**(6), 1260–1266 (2019).
18. Rauf, A., Abbas, Z. & Shehzad, S. A. Interactions of active and passive control of nanoparticles on radiative magnetohydrodynamics flow of nanofluid over oscillatory rotating disk in porous medium. *J. Nanofluids* **8**(7), 1385–1396 (2019).
19. Murthy, M. K. Numerical investigation on magnetohydrodynamics flow of Casson fluid over a deformable porous layer with slip conditions. *Indian J. Phys.* **2**, 1–10 (2020).
20. Oyelakin, I. S., Lalramneihmawii, P. C., Mondal, S., Nandy, S. K. & Sibanda, P. Thermophysical analysis of three-dimensional magnetohydrodynamic flow of a tangent hyperbolic nanofluid. *Eng. Rep.* **2**, 2 (2020).
21. Khashi'ie, N. S. *et al.* Magnetohydrodynamics (MHD) axisymmetric flow and heat transfer of a hybrid nanofluid past a radially permeable stretching/shrinking sheet with joule heating. *Chin. J. Phys.* **64**, 251–263 (2020).
22. Tlili, I., Nabwey, H. A., Ashwinkumar, G. P. & Sandeep, N. 3-D magnetohydrodynamic AA7072-AA7075/methanol hybrid nanofluid flow above an uneven thickness surface with slip effect. *Sci. Rep.* **10**(1), 1–13 (2020).
23. Khan, S. A., Khan, M. I., Hayat, T. & Alsaedi, A. Physical aspects of entropy optimization in mixed convective MHD flow of carbon nanotubes (CNTs) in a rotating frame. *Phys. Scr.* **94**(12), 125009 (2019).
24. Anuar, N. S., Bachok, N., Turkyilmazoglu, M., Arifin, N. M. & Rosali, H. Analytical and stability analysis of MHD flow past a nonlinearly deforming vertical surface in Carbon Nanotubes. *Alexandr. Eng. J.* **2**, 2 (2020).
25. Shah, Z., Bonyah, E., Islam, S. & Gul, T. Impact of thermal radiation on electrical mhd rotating flow of carbon nanotubes over a stretching sheet. *AIP Adv.* **9**(1), 015115 (2019).
26. Mahanthesh, B., Gireesha, B. J., Animasaun, I. L., Muhammad, T. & Shashikumar, N. S. MHD flow of SWCNT and MWCNT nanoliquids past a rotating stretchable disk with thermal and exponential space dependent heat source. *Phys. Scr.* **94**(8), 085214 (2019).
27. Anuar, N. S., Bachok, N., Arifin, N. M. & Rosali, H. MHD flow past a nonlinear stretching/shrinking sheet in carbon nanotubes: Stability analysis. *Chin. J. Phys.* **65**, 436–446 (2020).
28. Gul, T. *et al.* Magnetic dipole impact on the hybrid nanofluid flow over an extending surface. *Sci. Rep.* **10**(1), 1–13 (2020).
29. Ahmed, Z., Nadeem, S., Saleem, S. & Ellahi, R. Numerical study of unsteady flow and heat transfer CNT-based MHD nanofluid with variable viscosity over a permeable shrinking surface. *Int. J. Numer. Methods Heat Fluid Flow* **29**, 12 (2019).
30. Nagalakshm, P. S. S. & Vijaya, N. MHD flow of Carreau nanofluid explored using CNT over a nonlinear stretching sheet. *Front. Heat Mass Transfer* **14**, 2 (2020).
31. Tulu, A. & Ibrahim, W. MHD slip flow of CNT-ethylene glycol nanofluid due to a stretchable rotating disk with Cattaneo-Christov heat flux model. *Math. Probl. Eng.* https://doi.org/10.1155/2020/1374658 (2020).
32. Ghadikolaei, S. S. & Gholinia, M. 3D mixed convection MHD flow of GO-MoS2 hybrid nanoparticles in H2O–(CH2OH) 2 hybrid base fluid under the effect of H2 bond. *Int. Commun. Heat* https://doi.org/10.1016/j.icheatmasstransfer.2019.104371 (2020).
33. Acharya, N., Bag, R. & Kundu, P. K. Influence of Hall current on radiative nanofluid flow over a spinning disk: A hybrid approach. *Phys. E.* **111**, 103–112 (2019).
34. Veerakrishna, M. & Chamkha, A. J. Hall effects on unsteady MHD flow of second grade fluid through porous medium with ramped wall temperature and ramped surface concentration. *Phys. Fluids* https://doi.org/10.1063/1.5025542 (2018).
35. Abbasi, F. M., Gul, M. & Shehzad, S. A. Hall effects on peristalsis of boron nitrideethylene glycol nanofluid with temperature dependent thermal conductivity. *Phys. E Low-dimens. Syst. Nanostruct.* **99**, 275–284 (2018).
36. Mabood, F., Ibrahim, S. M., Rashidi, M. M., Shadloo, M. S. & Lorenzini, G. Non-uniform heat source/sink and Soret effects on MHD non-Darcian convective flow past a stretching sheet in a micropolar fluid with radiation. *Int. J. Heat Mass Transf.* **93**, 674–682 (2016).
37. Saba, F., Ahmed, N., Khan, U. & Mohyud-Din, S. T. A novel coupling of (CNT-Fe_3O_4/H_2O) hybrid nanofluid for improvements in heat transfer for flow in an asymmetric channel with dilating/squeezing walls. *Int. J. Heat Mass Transfer.* **136**, 186–195 (2019).
38. Yin, C., Zheng, L., Zhang, C. & Zhang, X. Flow and heat transfer of nanofluids over a rotating disk with uniform stretching rate in radial direction. *Propuls. Power Res.* **6**(1), 25–30 (2017).
39. Tassaddiq, A. *et al.* Heat and mass transfer together with hybrid nanofluid flow over a rotating disk. *AIP Adv.* **10**(5), 055317 (2020).

Author contributions

M.B. and M.A.K. wrote the original manuscript and performed the numerical simulations. M.S. reviewed the mathematical results and restructured the manuscript. Y.P.L., E.A.A., E.A. and M.G.A. revised the manuscript by checking the results with care. M.G.A., M.B., E.A. and M.A.K. checked the whole manuscript for validations of the mathematical and graphical results. All authors are agreed on the final draft of the submission file.

Competing interests

The authors declare no competing interests.

Additional information

Correspondence and requests for materials should be addressed to M.B.

Reprints and permissions information is available at www.nature.com/reprints.

Publisher's note Springer Nature remains neutral with regard to jurisdictional claims in published maps and institutional affiliations.